Chemical and electrochemical insertion of Li into the spinel structure of CuCr 2Se 4: Ex situ and in situ observations by X-ray diffraction and scanning electron microscopy

ARTICLE *in* PHYSICAL CHEMISTRY CHEMICAL PHYSICS · APRIL 2012

Impact Factor: 4.49 · DOI: 10.1039/c2cp00064d · Source: PubMed

8 AUTHORS, INCLUDING:

Wolfgang Bensch
Christian-Albrechts-Universität zu Kiel
727 PUBLICATIONS **6,476** CITATIONS
SEE PROFILE

Holger Gesswein
Karlsruhe Institute of Technology
32 PUBLICATIONS **173** CITATIONS
SEE PROFILE

Patric A. Gruber
Karlsruhe Institute of Technology
54 PUBLICATIONS **968** CITATIONS
SEE PROFILE

Sylvio Indris
Karlsruhe Institute of Technology
103 PUBLICATIONS **1,203** CITATIONS
SEE PROFILE

PCCP

Dynamic Article Links

Cite this: *Phys. Chem. Chem. Phys.*, 2012, **14**, 7509–7516

www.rsc.org/pccp

PAPER

Chemical and electrochemical insertion of Li into the spinel structure of $CuCr_2Se_4$: *ex situ* and *in situ* observations by X-ray diffraction and scanning electron microscopy

Wolfgang Bensch,*[a] Jannes Ophey,[a] Holger Hain,[b] Holger Gesswein,[c] Di Chen,[d] Reiner Mönig,[d] Patric A. Gruber[d] and Sylvio Indris[b]

Received 9th January 2012, Accepted 28th March 2012
DOI: 10.1039/c2cp00064d

The chemical and electrochemical insertion of lithium into the spinel structure of $CuCr_2Se_4$ was studied and the chemical reaction pathway was followed by *ex situ* X-ray diffraction on samples with different Li contents. The electrochemical reaction was investigated by *in situ* X-ray diffraction and *in situ* scanning electron microscopy. In the early steps of chemical intercalation, two phases with a different Li content coexist and Cu is extruded from the host material. After 4 days of Li intercalation, a conversion reaction is observed. The overall Li uptake is 8 Li ions per formula unit. The structural behaviour of the two intercalated phases at the early stages of intercalation is totally different. For one phase a strong expansion of the *a*-axis is observed while for the other phase it is only slightly affected by Li uptake. A three-step mechanism was found consisting of reduction of Se^- followed by a Cu–Li exchange and finally a complete reduction of Cr^{3+} to the metallic state accompanied by the formation of Li_2Se. The discharge capacity of the first cycle amounts to 530 mAh g^{-1} and drops to about 380 mAh g^{-1} in the fifth cycle. In *in situ* SEM images the occurrence of Cu whiskers that partially grow out of the crystallites can be observed.

Introduction

Intercalation chemistry is a mild method for the preparation of metastable materials which cannot be synthesized applying classical high-temperature routes. A large variety of host materials ranging from one-dimensional chain compounds to three-dimensional networks are able to host different guest atoms/ions or large molecules depending on the size of the empty sites to accommodate the guests and on the flexibility of the host structure.[1] In the case of conducting/semiconducting hosts, the reversible uptake and release of guests may be accompanied by a change in the charge density of the host materials: electrons are transferred from the guest to the host lattice during intercalation which are then removed during deintercalation reaction and both reactions lead to significant changes in the physical properties of the host–guest compounds.[2–18]

Besides the large synthetic potential of intercalation chemistry, the reversible insertion of Li into different host materials is the basis for the operation of rechargeable Li-ion batteries.[19–22] Many different materials have been tested and a variety of mechanisms can occur when Li reacts with the host material. Some layered structures allow topotactic intercalation of Li between the layers of the host material. The first material that was used for such studies was TiS_2[23] where Li can be inserted over a large range of concentrations leading to compositions Li_xTiS_2, $x = 0$–1. Nowadays commercial Li-ion battery cathode materials are based on $LiCoO_2$, where about half of the Li can be removed reversibly. These materials show good reversibility over a large number of intercalation cycles, but the specific charge/discharge capacities are limited, since at most one Li ion can be inserted/removed per transition metal ion, corresponding to oxidation/reduction between Co^{3+} and Co^{4+}.[21]

Another class of materials that are intensively studied are so-called conversion materials, where reversible Li insertion is based on the formation of new phases.[24] Much work has been done on binary compounds MX_m where reaction with Li takes place according to the equation

$$n\mathrm{Li} + \mathrm{MX}_m \rightarrow \mathrm{M} + n\mathrm{LiX}_{m/n} \quad (\mathrm{X} = \mathrm{O, S, F, H, N, Sb, P, \ldots})$$

These binary compounds include oxides (*e.g.* CoO,[25–30] Co_3O_4,[30,31] CuO,[25,32–34] Cu_2O,[32,35] NiO,[25,36] FeO,[25] α-Fe_2O_3,[37,38] γ-Fe_2O_3,[39] Fe_3O_4,[40] RuO_2,[41] Cr_2O_3,[42] WO_3[43]), sulfides (*e.g.* CuS,[44] Cu_2S,[44] FeS,[45] CoS,[45] MoS_2[46]), fluorides,[47] hydrides,[48] nitrides,[49] antimonides,[49,50] and phosphides.[50] The reduction of the metal

[a] *Institute of Inorganic Chemistry, University of Kiel, Olshausenstr. 40-60, 24098 Kiel, Germany. E-mail: wbensch@ac.uni-kiel.de*
[b] *Institute of Nanotechnology, Karlsruhe Institute of Technology, P.O. Box 3640, 76021 Karlsruhe, Germany*
[c] *Institute of Applied Materials (IAM-WPT), Karlsruhe Institute of Technology, P.O. BOX 3640, 76021 Karlsruhe, Germany*
[d] *Institute of Applied Materials (IAM-WBM), Karlsruhe Institute of Technology, P.O. BOX 3640, 76021 Karlsruhe, Germany*

ion M^{n+} to metallic M^0 is accompanied by the formation of the new phase Li_2O, Li_2S, LiF, *etc*. Equivalent mechanisms can also be found for more complex, *e.g*. ternary, compounds.

The advantage of these conversion materials is that *n*Li ions can be converted per metal atom M leading to theoretical specific capacities beyond 500 mAh g^{-1}. This is much higher than the values of nowadays commercial electrode materials like graphite (370 mAh g^{-1}) or $LiCoO_2$ (160 mAh g^{-1}). The disadvantage is that the formation of the new phase is accompanied by continuous formation of fresh interfaces as well as pronounced volume changes. These lead to irreversible loss of Li and to loss of contact to the current collector, respectively, and therefore to strong capacity fading during extensive cycling.

Bodenez *et al*. investigated the spinel systems $CuTi_2S_4$[51] and $CuCr_2S_4$.[51,52] A so-called CDI (combined displacement and intercalation) mechanism was found, similar to the reactions observed for the layer-structured materials $Cu_{2.33}V_4O_{11}$[53] and later also for $Sr_2MnO_2Cu_{2m-0.5}S_{m+1}$ (m = 1, 2, 3).[54]

The spinel systems Cu–(Ti/Cr)–(S/Se) are interesting because they allow the investigation of the effects of anion and cation substitution on the reaction mechanisms. Such substitutions can have a large influence on the diffusivity of the Li ions,[55] which is an important parameter for high-power batteries. While $CuTi_2S_4$ is a material with mixed cation valence (Ti^{3+}/Ti^{4+}),[51] $CuCr_2S_4$ reveals mixed anion valence ($S^{2-}/S^{-\bullet}$).[51,52]

In this line we investigated the ferromagnetic metallic spinel material $CuCr_2Se_4$ where the Cu^+ ions occupy tetrahedral sites and the Cr^{3+} ions are located on octahedral sites. From the electronic point of view, $CuCr_2Se_4$ is of special interest because charge neutrality is most likely achieved by the formation of a valence band hole and the formal charge balance situation can be described by the formula $[Cu^+][Cr_2{}^{3+}][Se_3{}^{2-}][Se^-]$. We note that there is a long debate in the literature about the real charge situation in $CuCr_2Se_4$ and several other models were proposed: $[Cu^{2+}][Cr^{3+}]_2[Se^{2-}]_4$,[56] $[Cu^+][Cr^{3+}Cr^{4+}][Se^{2-}]_4$[57] and $[Cu^+][Cr^{3+}{}_{1+\delta}Cr^{4+}{}_{1-\delta}][Se^{2-\delta}]_4$ with δ = 0.1.[58] On the basis of interatomic distances it was proposed that Cu is divalent in the chalcogenide spinels.[59] Even results of neutron scattering experiments were not conclusive and mixed covalent-metallic Cu–Se bonds were postulated to explain the observations. Moreover, for the ferromagnetic phase mixed-valent Cr^{3+}/Cr^{4+} was assumed, while in the paramagnetic region an oxidation state between +2 and +3 was postulated.[60] The Seebeck coefficient of the compound is positive indicating that holes are the dominating charge carriers.[61,62] In addition, band structure calculations demonstrated that the Se p states are largely but not completely filled.[63] Several interesting observations were also made in the past. The reversible topotactic redox reaction with Cu^+ leads to phases with composition $Cu_{1+y}Cr_2Se_4$ ($0 \le y \le 1$) being accompanied by a continuous decrease of the valence band hole concentration.[64,65] In $CuCr_2Se_4$ one Se can be replaced by Br^- without destroying the spinel structure leading to a semiconducting material.[66] In view of all these experimental and theoretical results the formal charge distribution with a valence band hole seems to be most likely. In any case, one should keep in mind that the assignment of oxidation states is a well established formalism in chemistry and is not a suitable tool to predict or explain the chemical bonding situation.

In order to understand the underlying reaction pathways that occur during insertion/extrusion of Li, it is necessary to use experimental techniques that can be applied *in situ* during chemical/electrochemical insertion/removal of Li. We used *in situ* X-ray diffraction (XRD) and *in situ* scanning electron microscopy (SEM) during electrochemical intercalation of Li into $CuCr_2Se_4$.

Experimental

The compound $CuCr_2Se_4$ was synthesized by high temperature reaction of the elements. In a typical run, 10 g of a stoichiometric mixture of Cu (−625 mesh, 99.9%, Alfa Aesar), Cr (−200 mesh, 99.95%, Alfa Aesar) and Se (−200 mesh, 99.999%, Alfa Aesar) were heated in an evacuated and sealed quartz ampoule for 28 days at 550 °C (heating rate: 20 °C h^{-1}). After the reaction, the ampoule was quenched in liquid nitrogen. The homogeneity of the samples was proved with XRD (Philips X'Pert diffractometer, CuK_α-radiation, reflection geometry) and subsequent Rietveld refinements. In addition, a chemical analysis was performed with inductively-coupled-plasma mass-spectrometry (ICP-MS) and all samples showed compositions very close to $CuCr_2Se_4$.

The first series of chemical intercalation reactions was performed in a glove-box using 330 mg of ground and sieved material (particle sizes: 20–33 μm). The powder was treated with a 1 : 1 mixture of *n*-hexane and 1.6 M *n*-butyllithium (*n*-BuLi, excess: 28 times) for 24, 48, 72 and 96 h at room temperature. A second series of reactions was done also at room temperature but using less Li excess. Four batches (0.8 mmol $CuCr_2Se_4$) were prepared and these batches were suspended in 0.5, 1, 1.5, and 2 mL of 1.6 M BuLi and 8 mL of *n*-hexane. The BuLi : $CuCr_2Se_4$ ratio was selected to give nominal compositions $Li_xCr_2Se_4$ with x = 1, 2, and 4. The mixtures were kept in a glove-box for 3 days. The Li content of the materials of both experiments was determined after the distinct reaction times using atomic absorption spectroscopy (AAS). Before AAS analysis all products were washed several times with *n*-hexane. All products were also investigated with XRD and partially further characterized with Rietveld refinements of the structures using the fundamental approach implemented in the TOPAS software.[67] Refined parameters: zero point, lattice parameters, *x*-coordinate of Se, background of the patterns, and Cu site occupancy in Cu deficient phases. The intercalated samples were prepared as flat samples using scotch tape as sample holder. All manipulations were done in a glove-box.

Electrochemical cycling was performed in coin cells using lithium metal foil as counter electrode. The electrode films were prepared on aluminium foil from a mixture of $CuCr_2Se_4$ (80%), polyvinylidene difluoride (10%), and carbon black (10%). The electrolyte was 1 M $LiPF_6$ in ethylene carbonate/dimethyl carbonate (EC/DMC, 1 : 1 weight ratio) and the separator was Celgard 2325 membrane (Celgard Inc, USA). The cells were tested using a Biologic VMP3 galvanostat. Galvanostatic cycling was performed at a C/200 rate (*i.e*. complete Li insertion within 200 hours) at voltages between 0.3 V and 4.0 V, and cyclovoltammograms were measured in the same voltage window at a sweep rate of 0.05 mV s^{-1}.

In situ XRD was performed in transmission cells[68] at the PDIFF beamline at the ANKA synchrotron in Karlsruhe operated at an energy of 12.49 keV (λ = 0.9933 Å). A wide angle position sensitive detector (Inel CPS 590) was used. This detector collects X-ray powder patterns within a few minutes covering an angle of 90° 2θ in 8192 channels simultaneously. The battery cell was discharged and charged continuously at a C/20 rate under constant current conditions and powder patterns were collected within 5 min acquisition time. The measurements were intensity corrected to account for the decay of the synchrotron beam between injection cycles. For a better signal-to-noise ratio two scans were summed prior to data analysis.

In situ SEM observations were made on special cells with electrode films deposited on a stainless steel mesh.[69] The counter electrode was Li metal, the separator was borosilicate filter paper (Whatman GF/B), and the electrolyte was a 0.5 M solution of Li–bis(trifluoromethanesulfonyl)imide (Li–TFSI) in Buthylmethylpyrrolidinium–TFSI (BMPyrr–TFSI) (Ionic Liquid Technologies GmbH, Heilbronn, Germany).

Results and discussion

Chemical reaction of $CuCr_2Se_4$ with *n*-BuLi

In Fig. 1 the X-ray powder patterns of the materials obtained after 1, 2, and 4 d treatment with *n*-BuLi are displayed. After 1 day a two-phase mixture is observed consisting of pristine material and intercalated $CuCr_2Se_4$. The Li content was determined to be 2.8 per formula unit and after 2 d the intercalation process is finished. With increasing reaction time significant changes of the powder patterns can be observed and after 4 d only little amount of intercalated $CuCr_2Se_4$ can be detected. Instead, new and broad reflections appeared which can be identified as Li_2Se and elemental Cu (Fig. 2). The AAS analysis of this sample yields about 8 Li per formula unit. From these results one can conclude that first an intercalation reaction occurs followed by extrusion of elemental Cu at a distinct Li content and finally the material is nearly completely converted. Interestingly, no reflections of elemental Cr can be observed in the powder pattern. This observation was also made for fully converted $CuCr_2S_4$.[51]

In the second series of experiments, the concentration of *n*-BuLi and $CuCr_2Se_4$ was chosen to give nominally stoichiometric $Li_xCuCr_2Se_4$ samples. The powder pattern of the compound with nominal x = 1 clearly shows two different phases. Additional reflections of elemental Cu are also visible. *In situ* X-ray diffraction performed on $Li_xCu_{1-x}Cr_2S_4$ showed the occurrence of the Cu(111) reflection at about $x \approx 0.3$–0.4.[51] It can be assumed that in the present system the critical composition is near this value. The results of the three-phase Rietveld refinement (Fig. 3) yield a $Li_xCuCr_2Se_4$ phase (phase 1) with a nearly identical a-axis compared to the pristine material (a = 10.31916(12) Å) and a second phase with a significantly enlarged a-axis (enlargement: 0.182 Å; see Table 1). The composition of phase 2 according to the site occupation factor obtained for Cu indicates a significant reduction of the Cu content to $Li_xCu_{0.5}Cr_2Se_4$. Within the limits of the Rietveld method the Cu content in phase 1 is not significantly reduced.

The powder pattern of the sample with nominal x = 2 (AAS: x = 1.86) contains also three different phases. The results of the Rietveld refinement (Fig. 4) indicate no significant change in the a-axis for phase 1 whereas the lattice parameter for phase 2 is reduced compared to that of $LiCuCr_2Se_4$. According to the refined Cu site occupation factors of both phases, the Cu content of phase 1 is comparable to that of the nominal $LiCuCr_2Se_4$ sample whereas the Cu content of phase 2 is further reduced yielding $Li_xCu_{0.4}Cr_2Se_4$ (Table 1).

The three-phase Rietveld refinement of the sample with the highest Li content (AAS: 3.92) is shown in Fig. 5. A small increase of the a-axis of phase 1 is observed whereas the lattice parameter of phase 2 further decreases (Table 1). While phase 1 contains a Cu content only slightly lower than that obtained for the other two samples mentioned above, the second phase contains a further reduced Cu content (Table 1). We note that

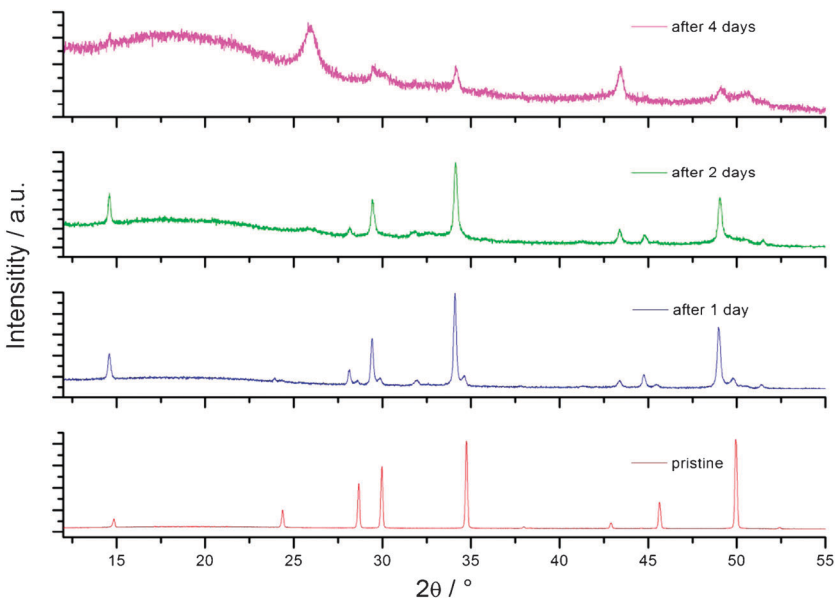

Fig. 1 X-ray powder patterns recorded after chemical intercalation, for several reaction times.

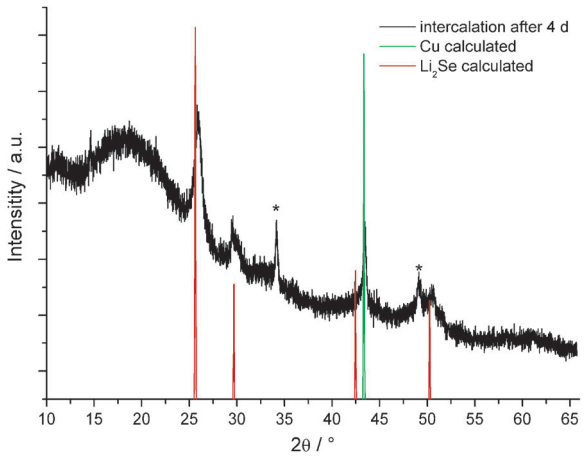

Fig. 2 X-ray powder pattern of the reaction product after the conversion process. Vertical lines indicate the Bragg positions of Cu and Li_2Se. Note: the broad modulation at around 20° 2θ is caused by the scotch tape and the two reflections not assigned (asterisks) are from remaining intercalated spinel.

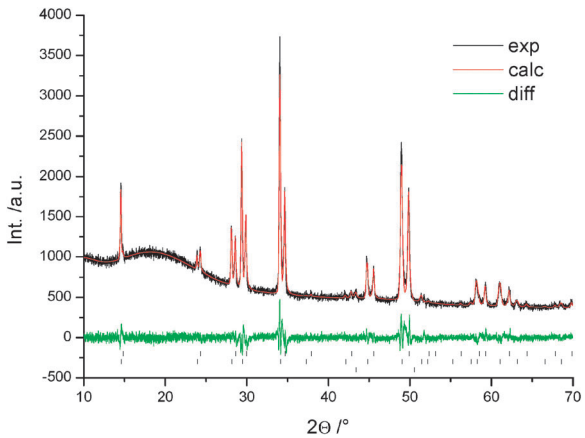

Fig. 3 Result of the Rietveld refinement of the sample with nominal composition $Li_1CuCr_2Se_4$. Black: measured powder pattern; red: refined profiles; vertical bars from top to bottom: phase 1, phase 2 and Cu. Note: the broad modulation at around 20° 2θ is caused by the scotch tape.

the compound is slightly contaminated by LiOH which was formed during preparation of the sample for the X-ray measurements.

The results of the structural analyses suggest the following model. Phase 2 exhibits an expansion of the lattice parameter upon Li^+ uptake compared to the pristine material, and a small enlargement of the *a*-axis of phase 1 is only observed for the sample with the highest Li content. The intercalated materials consist of two different phases with differing Li uptake capabilities, *i.e.* phase 1 seems to be less active and in the second phase most of the provided Li^+ is intercalated. During the intercalation process, Cu^+ is reduced to Cu and subsequently expelled from the sample. The slight increase of the *a*-axis of phase 1 with increasing nominal Li content and slightly decreasing Cu content suggests that Li^+ is also intercalated into this phase. The clear decrease of the *a*-axis of phase 2 with increasing Li content cannot be explained straightforwardly. The ionic radii of Li^+ and Cu^+ in tetrahedral coordination are 0.59 and 0.60 Å, respectively.[70] Hence, one would expect no significant

Table 1 Rietveld refinement results for the $Li_xCuCr_2Se_4$ samples with nominal x = 1, 2, and 4

	Phase 1	Phase 2	Cu
$Li_1CuCr_2Se_4$			
a/Å	10.3291(4)	10.5008(3)	3.607(1)
V/Å^3	1102.0(1)	1157.9(1)	
R_{wp}/%		5.25	
R_{exp}/%		3.91	
R_{Bragg}/%	2.07	3.17	2.66
Gof		1.342	
Refined Cu content	0.94(1)	0.51(1)	
Phase/%	43.5(2)	55.4(2)	1.0(2)
$Li_2CuCr_2Se_4$			
a/Å	10.3275(5)	10.4899(4)	3.607(1)
V/Å^3	1101.5(1)	1154.3(1)	
R_{wp}/%		5.59	
R_{exp}/%		3.57	
R_{Bragg}/%	3.20	3.20	0.37
Gof		1.564	
Refined Cu content	0.95(1)	0.41(1)	
Phase/%	23.0(2)	73.5(2)	3.5(2)
$Li_4CuCr_2Se_4$			
a/Å	10.372(1)	10.479(1)	3.608(1)
V/Å^3	1115.9(4)	1150.7(1)	
R_{wp}/%		3.42	
R_{exp}/%		2.35	
R_{Bragg}/%	1.0	2.38	0.85
Gof		1.453	
Refined Cu content	0.84(1)	0.19(1)	
Phase/%	48.2(4)	44.7(4)	7.1(2)

B_{iso} values of all atoms were fixed to 1.0. Gof: goodness of fit.

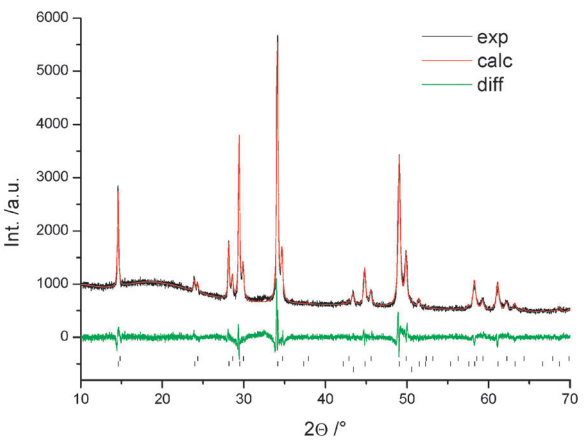

Fig. 4 Rietveld refinement result of the sample with nominal composition $Li_2CuCr_2Se_4$. Black: measured powder pattern; red: refined profiles; vertical bars from top to bottom: phase 1, phase 2 and Cu.

effect if Li^+ replaces Cu^+ in the host material. Assuming that Li^+ is exclusively located on octahedral sites, the maximum Li content would be 2 and, according to the ionic radii of Li^+ and Cu^+ in such coordination (Li^+: 0.76 Å; Cu^+: 0.77 Å[70]), this should lead to no significant change of the lattice parameter. But for phase 2 first an expansion of about 0.18 Å is observed for the sample with nominal composition $LiCuCr_2Se_4$ compared to the pristine material despite removal of Cu from the host lattice. We note that for $CuCr_2S_4$ an expansion of the lattice parameter was also observed upon Li uptake.[51] According to a combined refinement of neutron powder diffraction and X-ray diffraction data performed on fully discharged $Li_xCuCr_2S_4$

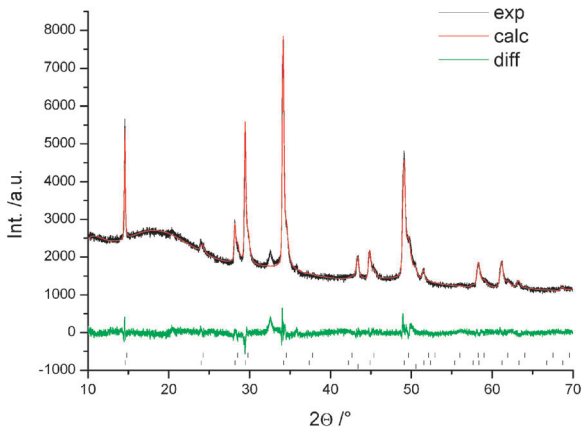

Fig. 5 Rietveld refinement result of the sample with nominal composition $Li_4CuCr_2Se_4$. Black: measured powder pattern; red: refined profiles; vertical bars from top to bottom: phase 1, phase 2 and Cu. The peak at 32.5° belongs to LiOH impurity.

(composition: $Li_{1.75}Cu_{0.25}Cr_2S_4$), Li^+ ions exclusively occupy the octahedral 16c site[52] despite face-sharing of the octahedra with the tetrahedra hosting Cu^+. Due to the expulsion of 75% Cu^+ the energetically unfavorable Cu^+–Li^+ situation is sufficiently reduced. On the basis of these results one can assume that a similar structural situation is realized in the present host material.

The first electron transferred to the host material may eliminate the valence band hole, *i.e.* the formally present Se^- is reduced to Se^{2-}. Because the ionic radius of Se^{2-} is larger than that of Se^-, the expansion may be explained on this basis. Further increase of the nominal Li content in the material leads to a moderate decrease of the *a*-axis for phase 2. Because more Cu is expelled from the host, the expansion of the lattice is overcompensated by the loss of Cu. For the sample with nominal composition $Li_4CuCr_2Se_4$ the two phases host in sum about 4 Li^+ cations and without knowledge of the location of Li^+ in the structures one can only speculate about the real structural situation.

Electrochemical reaction of $CuCr_2Se_4$ with Li

Fig. 6 shows the voltage profile during the first two cycles of galvanostatic cycling of $CuCr_2Se_4$ against a Li metal counter electrode. During the first discharge, two major processes are visible. The first process occurs at voltages between 2.0 V and 1.0 V and the fine structure in the profile hints at multiple reaction steps. The length of this plateau corresponds to insertion of 2 Li ions per formula unit $CuCr_2Se_4$. Subsequently, a long plateau at about 1.0 V appears and its length corresponds to insertion of six more Li ions. At potentials below 0.9 V, contributions due to formation of the so-called solid–electrolyte interphase occur resulting in *irreversible* capacity losses. The overall *reversible* Li uptake is 8 Li ions per formula unit and equals the maximum Li uptake obtained during chemical reaction with BuLi, being accompanied by a conversion of the material. The first charge profile reveals similar features, *i.e.* a plateau at about 1.7 V and subsequently a process between 1.7 V and 2.5 V. The voltage profile of the second cycle (dashed line) resembles that of the first cycle. While the

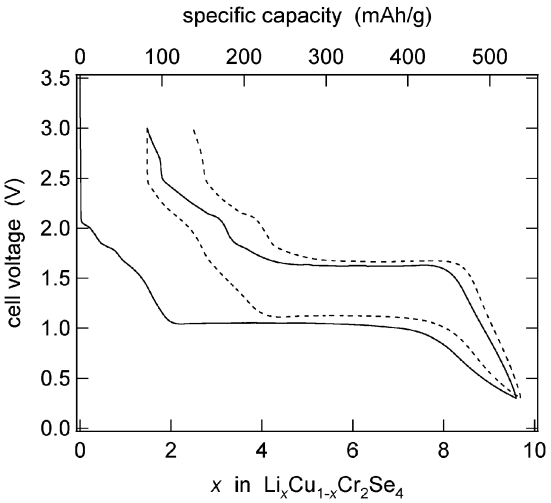

Fig. 6 Voltage profile during first (solid line) and second (dashed line) cycle of galvanostatic cycling of $CuCr_2Se_4$ against a Li metal counter electrode.

discharge capacity of the second cycle equals the charge capacity of the first cycle, clear losses occur during the first and second charging, *i.e.* during re-oxidation of the host material.

The cyclovoltammogram of $CuCr_2Se_4$ against a Li metal counter electrode (Fig. 7) shows reduction and oxidation peaks that correspond to the plateau values shown in Fig. 6. One of the reduction processes exhibits a shift from the first cycle (about 0.8 V) to the second cycle (1.0 V). In the following cycles (not shown here), the position of this peak is constant, although some broadening may be caused by an increase of structural disorder.

The discharge and charge capacities of $CuCr_2Se_4$, when cycled at a rate of C/200 (*i.e.* complete discharge within 200 h) against the Li metal, are displayed in Fig. 8 for the first 5 cycles. The capacities exhibit a decrease from 530 mAh g^{-1} to 380 mAh g^{-1}, but also stabilization at this value. Again it can be seen that the discharge capacities are very close to the charge capacities of the preceding cycle, and that the losses occur mainly during charging.

The different phases that occur during electrochemical insertion of Li into $CuCr_2Se_4$ were observed by *in situ* XRD. Fig. 9 shows the XRD scans acquired during discharging $CuCr_2Se_4$ against

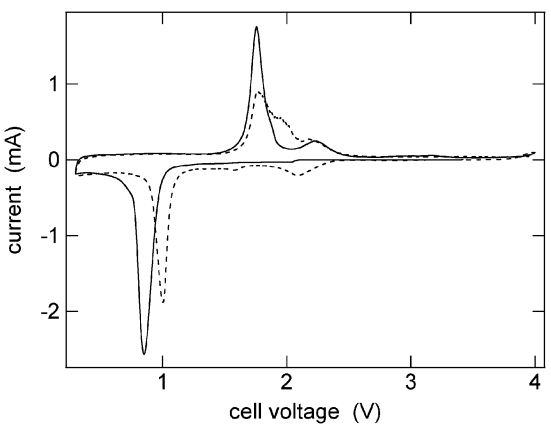

Fig. 7 First (solid line) and second (dashed line) cycle of cyclovoltammogram of $CuCr_2Se_4$ cycled against a Li metal counter electrode.

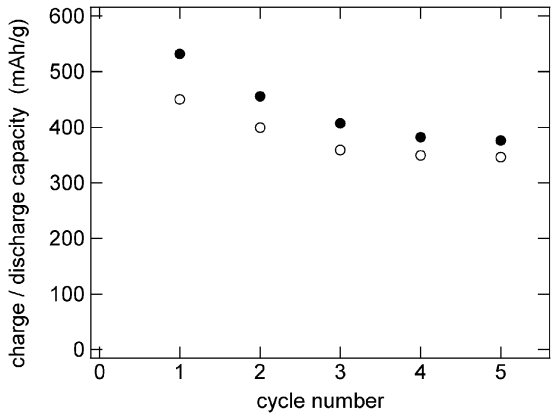

Fig. 8 Discharge (full circles) and charge (empty circles) capacities of $CuCr_2Se_4$ cycled against a Li metal counter electrode with a rate of C/200.

a Li metal electrode. The peak splitting of the (400) and (440) reflections of $CuCr_2Se_4$ clearly shows the disappearance of the initial spinel phase and the formation of a new, Li-rich spinel phase with a larger cubic lattice constant. This peak splitting and peak shift to smaller 2θ values are accompanied with peak broadening which indicates the development of inhomogeneous microstrain during Li intercalation and the decrease of the intensity of the reflections of the host material indicates conversion of the material. At the end of the discharge process only small amounts of intercalated spinel phase can be detected in the powder pattern. The presence of small amounts of the spinel phase after full discharge can be explained by the quite fast cycling during this *in situ* experiment (C/20 instead of C/200, *cf.* Fig. 6). The phase change is accompanied by the formation of Cu metal particles as can be seen by the appearance of the copper (111) peak at 27.56° 2θ. This suggests that the first step in the electrochemical reaction, visible in the voltage profile at voltages between 2.0 V and 1.0 V (Fig. 6), includes a Cu–Li exchange reaction, where most of the Cu^+ is replaced by 2 Li^+, resulting in a phase with nominal composition $Li_2Cu_{1-x}Cr_2Se_4$. At the end of the discharge reaction, the presence of Li_2Se becomes apparent. This reveals that the

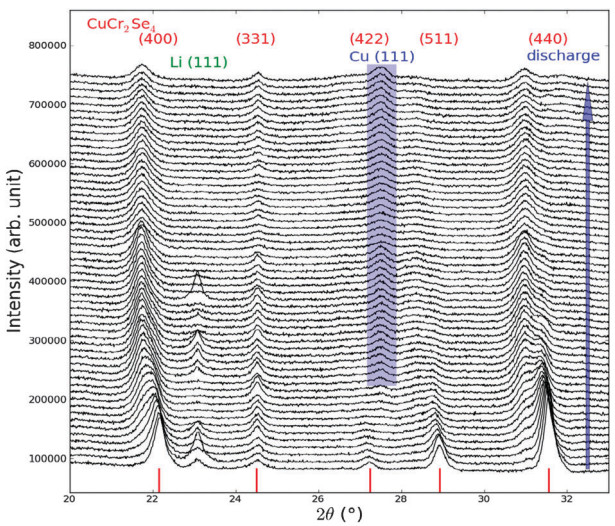

Fig. 9 *In situ* XRD scans recorded during electrochemical insertion of Li into $CuCr_2Se_4$.

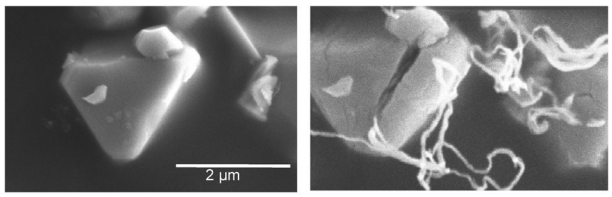

Fig. 10 *In situ* SEM observation of the $CuCr_2Se_4$ particles during electrochemical insertion of Li (both micrographs are taken with same magnification).

second step, which is represented in the voltage profile by a long plateau at 1.0 V, corresponds to insertion of six additional Li ions per formula unit $CuCr_2Se_4$ (Fig. 6), *i.e.*, a complete reduction of 2 Cr^{3+} to the metallic state occurs. These findings are consistent with the results obtained from *ex situ* XRD on samples after chemical Li insertion from BuLi.

Fig. 10 shows *in situ* SEM micrographs of $CuCr_2Se_4$ particles obtained during electrochemical insertion of Li. Note that in this *in situ* SEM investigation the *same* crystals are observed at different reaction times. A significant increase of the particle size is observed that finally leads to cracking of these particles. This is accompanied by the formation of whiskers that partially grow out of these cracks. Comparison with the *in situ* XRD results suggests that these are Cu metal whiskers.

In the literature, several transition metal sulfides or oxides were studied with respect to the reaction mechanism and the electrochemical behaviour upon Li uptake, while studies using selenide host lattices are very rare. Hence, a short comparison is presented for the isostructural compound $CuCr_2S_4$, CrS and CuS. The spinel $CuCr_2S_4$ behaves similar to the selenide investigated here. Discharge to 0.02 V is accompanied by the uptake of 8 Li and a full conversion to Cu, Cr and Li_2S.[51] After intercalation of about 0.4 Li in $Li_xCuCr_2S_4$, a new phase $Li_{2-x}Cu_{0.3}Cr_2S_4$ appeared together with extrusion of elemental Cu. Before the conversion reaction starts, the composition of the material is $Li_{1.75}Cu_{0.25}Cr_2S_4$. During the charging process about 7 Li could be removed from the converted material,[51] being comparable with the results presented here. For CrS a conversion reaction was observed at a voltage of 0.85 V leading to the formation of metallic Cr in a Li_2S matrix.[45] Up to about 1.8 Li per formula unit could be inserted during the discharge cycle leading to a specific capacity of about 650 mAh g^{-1}. CuS showed an interesting behaviour during Li uptake and removal. During the discharge process, first the formation of an intermediate $Cu_{2-x}S$ phase occurs which then undergoes a displacement, rather than a conversion reaction. Large Cu dendrites are then formed surrounding the Li_2S matrix. In the charging cycle the dendrites disappeared, and Cu re-entered the matrix creating massive particles of $Cu_{2-x}S$ and finally CuS. However, the specific capacity of the Li/$Cu_{2-x}S$ system dropped from about 650 mAh g^{-1} to less than ~100 mAh g^{-1} within two cycles.[44]

It seems that Cu containing chalcogenides behave different from other compounds with respect to the reaction mechanism. The three samples CuS, $CuCr_2S_4$, and $CuCr_2Se_4$ undergo a copper extrusion reaction at a distinct Li content followed by a conversion of the materials to metallic elements embedded in the Li_2X matrix (X = S, Se).

Conclusions

Li could be inserted into the spinel structure of $CuCr_2Se_4$ by chemical and electrochemical methods. During chemical intercalation two Li containing phases coexist and at a distinct Li concentration elemental Cu is formed. We showed by electrochemical cycling that the Li insertion is reversible and that overall 8 Li ions could be inserted per formula unit which corresponds to a subsequent reduction of Cu^{+}, $Se^{-\bullet}$, and $2Cr^{3+}$ accompanied by the formation of Li_2Se and elemental Cr and Cu. The insertion of Li leads to changes in the lattice parameters but also to the formation of internal strain.

Acknowledgements

We are grateful to the German Federal Ministry of Education and Research for financial support. We also thank ANKA for beamtime allocation.

References

1 *Intercalation Chemistry*, M. S. Whittingham and A. J. Jacobson, Academic Press, New York, 1984.
2 J. M. Tarascon, F. J. DiSalvo, M. Eibschütz, D. W. Murphy and J. V. Waszczak, *Phys. Rev. B*, 1983, **28**, 6397–6406.
3 H. Narita, H. Ikuta, H. Hinode, T. Uchida, T. Ohtani and M. Wakihara, *J. Solid State Chem.*, 1994, **108**, 148–151.
4 T. Ohtani, A. Tsubot and K. Oshima, *Mater. Res. Bull.*, 1999, **34**, 1143–1152.
5 R. Brec, E. Prouzet and G. Ouvrard, *J. Power Sources*, 1993, **43–44**, 277–288.
6 C. N. Field, M.-L. Boillot and R. Clément, *J. Mater. Chem.*, 1998, **8**, 283–284.
7 D. O'Hare, H.-V. Wong, S. Hazell and J. W. Hodby, *Adv. Mater.*, 1992, **4**, 658–660.
8 V. Sanchez, E. Benavente, M. A. Santa Ana and G. Gonzalez, *Chem. Mater.*, 1999, **11**, 2296–2298.
9 D. Qian, D. Hsieh, L. Wray, Y. Xia, R. J. Cava, E. Morosan and M. Z. Hasan, *Phys. B*, 2008, **403**, 1002–1004.
10 W. Bensch, J. Koy and W. Biberacher, *Solid State Commun.*, 1995, **93**, 261–264.
11 W. Bensch, O. Helmer and M. Muhler, *J. Alloys Compd.*, 1997, **246**, 62–69.
12 W. Bensch, B. Sander, O. Helmer, C. Näther, F. Tuczek, A. Panich and A. Shames, *J. Solid State Chem.*, 1999, **145**, 235–246.
13 W. Bensch, O. Helmer, C. Näther and M. Muhler, *J. Solid State Chem.*, 1999, **145**, 247–252.
14 M. Behrens, O. Riemenschneider, W. Bensch, S. Indris, M. Wilkening and P. Heitjans, *Chem. Mater.*, 2006, **18**, 1569–1576.
15 M. Behrens, R. Kiebach, J. Ophey, O. Riemenschneider and W. Bensch, *Chem.–Eur. J.*, 2006, **12**, 6348–6355.
16 J. Wontcheu, M. Behrens, W. Bensch, S. Indris, M. Wilkening and P. Heitjans, *Solid State Ionics*, 2007, **178**, 759–768.
17 M. Behrens, J. Wontcheu, R. Kiebach and W. Bensch, *Chem.–Eur. J.*, 2008, **14**, 5021–5029.
18 S. Indris, J. Wontcheu and W. Bensch, *Phys. Chem. Chem. Phys.*, 2009, **11**, 3250–3256.
19 *Handbook of Batteries*, ed. D. Linden and T. B. Reddy, McGraw-Hill, New York, 1995.
20 *Advances in Lithium-Ion Batteries*, ed. W. A. van Schalkwijk and B. Scrosati, Kluwer Academic, New York, 2002.
21 *Lithium Batteries—Science and Technology*, ed. G.-A. Nazri and G. Pistoia, Kluwer Academic, Boston, 2004.
22 J. Wontcheu, W. Bensch, M. Wilkening, P. Heitjans, S. Indris, P. Sideris, C. P. Grey, S. Mankovsky and H. Ebert, *J. Am. Chem. Soc.*, 2008, **130**, 288–299.
23 M. S. Whittingham, *Prog. Solid State Chem.*, 1978, **12**, 41–111.
24 J. Cabana, L. Monconduit, D. Larcher and M. R. Palacín, *Adv. Energy Mater.*, 2010, **22**, E170–E192.
25 P. Poizot, S. Laruelle, S. Grugeon and J.-M. Tarascon, *J. Electrochem. Soc.*, 2002, **149**, A1212–A1217.
26 S. Laruelle, S. Grugeon, P. Poizot, M. Dolle, L. Dupont and J.-M. Tarascon, *J. Electrochem. Soc.*, 2002, **149**, A627–A634.
27 Y. Yu, C. H. Chen, J.-L. Shui and S. Xie, *Angew. Chem., Int. Ed.*, 2005, **44**, 7085–7089.
28 Y. Yu, Y. Shi and C.-H. Chen, *Chem.–Asian J.*, 2006, **1**, 826–831.
29 J.-S. Do and C.-H. Weng, *J. Power Sources*, 2006, **159**, 323–327.
30 G. X. Wang, Y. Chen, K. Konstantinov, M. Lindsay, H. K. Liu and S. X. Dou, *J. Power Sources*, 2002, **109**, 142–147.
31 Y.-M. Kang, M.-S. Song, J.-H. Kim, H.-S. Kim, M.-S. Park, J.-Y. Lee, H. K. Liu and S. X. Dou, *Electrochim. Acta*, 2005, **50**, 3667–3673.
32 S. Grugeon, S. Laruelle, R. Herrera-Urbina, L. Dupont, P. Poizot and J.-M. Tarascon, *J. Electrochem. Soc.*, 2001, **148**, A285–A292.
33 A. Debart, L. Dupont, P. Poizot, J.-B. Leriche and J.-M. Tarascon, *J. Electrochem. Soc.*, 2001, **148**, A1266–A1274.
34 J. Morales, L. Sanchez, F. Martin, J. R. Ramos-Barrado and M. Sanchez, *Thin Solid Films*, 2005, **474**, 133–140.
35 Y. Yu, Y. Shi and C.-H. Chen, *Nanotechnology*, 2007, **18**, 055706 (5pp).
36 B. Varghese, M. V. Reddy, Z. Yanwu, C. S. Lit, T. C. Hoong, G. V. S. Rao, B. V. R. Chowdari, A. T. S. Wee, C. T. Lim and C.-H. Sow, *Chem. Mater.*, 2008, **20**, 3360–3367.
37 D. Larcher, C. Masquellier, D. Bonnin, Y. Chabre, V. Masson, J.-B. Leriche and J.-M. Tarascon, *J. Electrochem. Soc.*, 2003, **150**, A133–A139.
38 P. C. Wang, H. P. Ding, T. Bark and C. H. Chen, *Electrochim. Acta*, 2007, **52**, 6650–6665.
39 S. Kanzaki, T. Inada, T. Matsumura, N. Sonoyama, A. Yamada, M. Takano and R. Kanno, *J. Power Sources*, 2005, **146**, 323–326.
40 P. L. Taberna, S. Mitra, P. Poizot, P. simon and J.-M. Tarascon, *Nat. Mater.*, 2006, **5**, 567–573.
41 P. Balaya, H. Li, L. Kienle and J. Maier, *Adv. Funct. Mater.*, 2003, **13**, 621–625.
42 L. Dupont, S. Laruelle, S. Grugeon, C. Dickinson, W. Zhou and J.-M. Tarascon, *J. Power Sources*, 2008, **175**, 502–509.
43 A. C. Dillon, A. H. Mahan, R. Deshpande, P. A. Parilla, K. M. Jones and S.-H. Lee, *Thin Solid Films*, 2008, **516**, 794–797.
44 A. Debart, L. Dupont, R. Patrice and J.-M. Tarascon, *Solid State Sci.*, 2006, **8**, 640–651.
45 Y. Kim and J. B. Goodenough, *J. Phys. Chem. C*, 2008, **112**, 15060–15064.
46 R. Dominko, D. Arcon, A. Mrzel, A. Zorko, P. Cevc, P. Venturini, M. Gaberscek, M. Remskar and D. Mihailovic, *Adv. Mater.*, 2002, **14**, 1531–1534.
47 G. G. Amatucci and N. Pereira, *J. Fluorine Chem.*, 2007, **128**, 243–262.
48 Y. Oumellal, A. Rougier, G. A. Nazri, J.-M. Tarascon and L. Aymard, *Nat. Mater.*, 2008, **7**, 916–921.
49 R. Malini, U. Uma, T. Sheela, M. Ganesan and N. G. Renganathan, *Ionics*, 2009, **15**, 301–307.
50 J. F. Tirado, *Mater. Sci. Eng.*, 2003, **R40**, 03–136.
51 V. Bodenez, L. Dupont, M. Morcrette, C. Surcin, D. W. Murphy and J.-M. Tarascon, *Chem. Mater.*, 2006, **18**, 4278–4287.
52 V. Bodenez, L. Dupont, L. Laffont, A. R. Armstrong, K. M. Shaju, P. G. Bruce and J.-M. Tarascon, *J. Mater. Chem.*, 2007, **17**, 3238–3247.
53 M. Morcrette, P. Rosier, L. Dupont, E. Mugnier, L. Sannier, J. Galy and J.-M. Tarascon, *Nat. Mater.*, 2003, **2**, 755–761.
54 S. Indris, J. Cabana, O. J. Rutt, S. J. Clarke and C. P. Grey, *J. Am. Chem. Soc.*, 2006, **128**, 13354–13355.
55 W. Bensch, T. Bredow, H. Ebert, P. Heitjans, S. Indris, S. Mankovsky and M. Wilkening, *Prog. Solid State Chem.*, 2009, **37**, 206–225.
56 J. B. Goodenough, *Solid State Commun.*, 1967, **5**, 577–580.
57 F. K. Lotgering, *Proc. Int. Conf. on Magnetism*, Nottingham, 1964, p. 533.
58 F. K. Lotgering and R. P. van Stapele, *J. Appl. Phys.*, 1968, **39**, 417–423.
59 A. W. Sleight, *Mater. Res. Bull.*, 1967, **12**, 1107–1109.
60 D. Rodic, B. Antic, R. Tellgren, H. Rundlof and J. Blanusa, *J. Magn. Magn. Mater.*, 1998, **187**, 88–92.
61 G. J. Snyder, T. Caillat and J.-P. Fleurial, *Mater. Res. Innovations*, 2001, **5**, 67–73.

62 M. Robbins, H. W. Lehmann and J. G. White, *J. Phys. Chem. Solids*, 1967, **28**, 897–902.
63 J. S. Bettinger, R. V. Chopdekar, M. Liberati, J. R. Neulinger, M. Chshiev, Y. Takamura, L. M. B. Alldredge, E. Arenholz, Y. U. Idzerda, A. M. Stacy, W. H. Butler and Y. Suzuki, *J. Magn. Magn. Mater*., 2007, **318**, 65–73.
64 R. Schöllhorn and A. Payer, *Angew. Chem*., 1986, **98**, 895–897 (*Angew. Chem., Int. Ed. Engl*., 1986, **25**, 905).
65 A. Payer, R. Schöllhorn, C. Ritter and W. Paulus, *J. Alloys Compd*., 1993, **191**, 37–42.
66 A. Payer, M. Schmalz, W. Paulus, R. Schöllhorn, R. Schlögl and C. Ritter, *J. Solid State Chem*., 1992, **98**, 71–81.
67 A. Coelho, *Topas Academic*, Coelho Software, Brisbane, Australia, 4.1 edn, 2007.
68 M. Balasubramanian, X. Sun, X. Q. Yang and J. McBreen, *J. Power Sources*, 2001, **92**, 1–8.
69 D. Chen, S. Indris, M. Schulz, B. Gamer and R. Mönig, *J. Power Sources*, 2011, **196**, 6382–6387.
70 R. D. Shannon, *Acta Crystallogr., Sect. A: Cryst. Phys., Diffr., Theor. Gen. Crystallogr*., 1976, **A32**, 751–767.

